A Uniform GTD Treatment of Surface Diffraction by Impedance and Coated Cylinders

Paul E. Hussar, *Member, IEEE*

***Abstract*—In the context of the uniform geometrical theory of diffraction (UTD), computation of the scattered fields near the shadow boundary of a smooth convex surface requires values for the Pekeris-integral function $p^*(\xi, q)$. While in a small number of cases such as the case of perfect conductivity ($q = 0$ and $q \to \infty$), tabulated values of the function are available; in the general case, these values must be obtained by some numerical method. Here, a procedure for approximating $p^*(\xi, q)$ by residue-series means will be introduced. In contrast with traditional residue-series representations, the new procedure requires only a limited knowledge of pole locations even in the shadow boundary transition region and thereby extends the regime of practical applicability of residue-series methods beyond the deep shadow. It will be demonstrated that the new procedure can be combined with an earlier residue-series representation derived by this author and R. Albus (and with geometrical optics) to provide a computationally efficient procedure for computing fields scattered by an impedance or coated cylinder.**

***Index Terms*—Geometrical theory of diffraction.**

I. Introduction

DEVELOPMENTS in materials science and the advancement of low-observability techniques have created a requirement for high-frequency scattering analysis techniques that are applicable in cases where the scattering surfaces are not perfect conductors. In order to address this requirement, various authors [1]–[3] have discussed the two-dimensional problem of scattering by a cylinder whose surface is either coated or characterized by an impedance boundary condition (IBC). A fundamental objective has been to introduce into solutions for impedance/coated-cylinder problems the kind of simplicity and computational efficiency that is, in the case of perfectly conducting scatterers associated with the uniform geometrical theory of diffraction (UTD) [4]. As extensions of [4], [1]–[3] must address field approximation in each of three roughly distinct regions (see [3], in particular). In the illuminated region far from the shadow boundary (i.e., the deep-lit region) a reflected-field component can be quickly and accurately evaluated via geometrical optics (GO). In the deep shadow, a representation in terms of Keller-type modes [5] is required in order to permit geometrical theory of diffraction (GTD)-type generalization from the circular-cylinder case to cases of nonconstant cylinder curvature. Finally, in the vicinity of the shadow boundary (i.e., the transition region), neither GO nor the Keller-modal representations employed in [1]–[3] are adequate (the latter, in particular, diverge at the shadow boundary). Instead, field computation is based on the UTD transition-region representation and surface properties are taken into account by employing an appropriate transition integral in Pekeris-function form [6]–[8].

While tabulated Pekeris integral values are available in the case of perfect conductivity, no such values can be expected to be available in the general case. To overcome this limitation, a method for optimizing the efficiency of numerical Pekeris-integral evaluation has been obtained by Pearson [9]. Alternatively, Kim and Wang [1], [2] have explored a heuristic means for evaluating the Pekeris integral function. Employment of either of these methods involves implementation of a second numerical procedure in addition to the identification of pole locations required by a Keller-type modal-series representation of the deep-shadow-region fields.

The purpose of the present paper is to introduce a general procedure whereby the transition-region fields scattered by an impedance or coated cylinder can be efficiently approximated using the same pole locations as are employed within the deep-shadow region. While residue-series expressions have been used before to represent the fields in the transition region [10], [11], the new procedure is distinguished by the fact that it permits the number of residue-series terms required for convergence in the transition region to be fixed at some modest value that is independent of the problem geometry. The argument that will be advanced on behalf of the new procedure relies heavily on results from [10] in which a novel shadow-region residue-series solution for the line-source and conducting-cylinder canonical problem is described. The solution from [10] (and here adapted to impedance and coated cylinders) can be written in terms of GTD ray coordinates and, unlike the cylinder solution employed by Keller, converges at the shadow boundary. This solution will undergo a slight reworking that will lead to the introduction of a new function designated as $p^*(\xi, q, u)$ and defined for negative (lit region) as well as positive (shadow region) values of ξ. The motivation for introducing this new function is that while the solution from [10] converges slowly at the shadow boundary when the source and observation point are remote from the scatterer, use of $p^*(\xi, q, u)$ near $\xi = 0$ permits a Pekeris-type transition integral [denoted as $p^*(\xi, q)$] to be approximated from a modest number of residue-series terms. Computation of the transition-region fields via the new procedure occurs first via residue-series evaluation of $p^*(\xi, q, u)$ and then via the familiar UTD formulas with $p^*(\xi, q, u)$ employed as an approximation for the Pekeris integral.

Manuscript received August 16, 1996; revised July 7, 1997.
The author is with IIT Research Institute, Annapolis, MD 21401 USA.
Publisher Item Identifier S 0018-926X(98)05776-7.

The outstanding consequence of the new procedure, namely that the transition-region fields, can readily be computed from knowledge of a limited number of pole locations and should not be seen as being in conflict with accepted notions about the behavior of residue-series solutions to familiar canonical problems. Rather, the new procedure should be viewed as taking advantage of a notable feature of the UTD format, namely that the single function $p^*(\xi, q)$, which depends on geometry only through ξ, characterizes scattering by a given cylinder over a large domain of source/observation-point configurations. The new function $p^*(\xi, q, u)$ can be interpreted as a piece extracted from the residue-series solution in [10] that, within the transition region, exhibits in an approximate way the same property as $p^*(\xi, q)$. This new function will be seen (for small ξ) to asymptotically approach $p^*(\xi, q)$ as the value of the argument u is increased beyond unity. Efficient approximation of $p^*(\xi, q)$ occurs via evaluation of $p^*(\xi, q, u)$ with u chosen close to unity whereupon, as will be demonstrated, rapid residue-series convergence is assured.

As the deep-lit region is approached (i.e., ξ assumes a large negative value), the asymptotic approach of $p^*(\xi, q, u)$ to $p^*(\xi, q)$ occurs more slowly than for ξ near zero and approximation of $p^*(\xi, q)$ with $p^*(\xi, q, u)$ for u close to unity becomes less accurate. A heuristic interpolation scheme has been implemented to allow the GO reflection coefficient to be recovered smoothly as the deep-lit region is entered. The situation for positive ξ is less problematic. A modal representation having the form described in [10] can be smoothly joined with the new transition-region representation at positive ξ chosen in such a way that the large numbers of residue-series terms that appear in [10] never arise. The overall result that will be demonstrated is that the entire scattered field can be determined from as few as ten pole locations without regard for the problem geometry.

Distinct treatments will separately be provided for the case where a simple IBC is applied at the cylinder surface and for the case where a perfectly conducting cylinder is coated by a single layer of dielectric/magnetic material. These two formulations exhibit considerable overlap in terms of applicability, and their relative merits will, therefore, be indicated. The overall methodology described in this paper should not, however, be understood as being limited to these two cases. Rather, extension of the new procedure to further cases can be expected to be straightforward as comparison between the formulations here provided will illustrate.

In Section II, a shadow-region uniform GTD solution for a line source radiating in the vicinity of an infinitely long circular cylinder characterized by a constant surface impedance is developed via a method analogous to that employed in [10] for the conducting case. It is shown that this solution can be rewritten in a format identical to that of the UTD solution except that $p^*(\xi, q)$ becomes replaced by $p^*(\xi, q, u_g)$, where u_g is a geometry-specific value of the argument u. Because, in the transition region, the problem-geometry-dependence through u_g is weak, it becomes possible to replace u_g with another, "optimal" argument value chosen close to unity to ensure that $p^*(\xi, q, u)$ can be efficiently evaluated. To extend this approach to the lit region, the form of $p^*(\xi, q, u)$ for negative ξ must be determined by analytic continuation. Equivalent results for the coated cylinder are obtained in Section III, except that certain approximations employed in the Section II formulation, as well as the accompanying limitations, are avoided. Implementation of the results obtained in Sections II and III is described in Section IV. That, for small ξ, $p^*(\xi, q, u)$ rapidly approaches $p^*(\xi, q)$ in the transition region as u grows larger than unity is demonstrated with some examples. A smooth concatenation of impedance and coated-cylinder transition-region solutions with solutions applicable to other regions is obtained heuristically from examination of $p^*(\xi, q, u)$ data. Eigenfunction series results are then employed to assess the accuracy of a complete uniform GTD solution that is based on $p^*(\xi, q, u)$ in the transition region, GO in the deep-lit region and the impedance/coated cylinder implementation of [10] in the deep shadow.

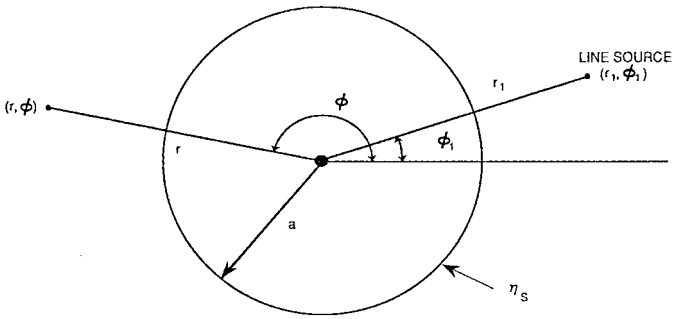

Fig. 1. Geometry for the line-source and impedance-cylinder problem.

II. Impedance Cylinder

The uniform GTD methods that will be described in this paper rely, ultimately, on the availability of the residue-series format for representing the shadow-region fields. Consider, therefore, a unit electric or magnetic line source radiating in the vicinity of an infinitely long circular cylinder with surface impedance η_s (see Fig. 1). At the surface of the cylinder $(r = a)$ the applicable boundary conditions are $H_\phi = E_z/\eta_s$ for the TM case and $E_\phi = -\eta_s H_z$ for the TE case. It is more convenient to write these boundary conditions as

$$\frac{\partial E_z}{\partial r} - jkC_{\mathrm{TM}}E_z = 0 \tag{1a}$$

for the TM fields and

$$\frac{\partial H_z}{\partial r} - jkC_{\mathrm{TE}}H_z = 0 \tag{1b}$$

for the TE fields where $k = \omega(\mu_0\varepsilon_0)^{1/2}$, $C_{\mathrm{TE}} = \eta_s/\eta_0, C_{\mathrm{TM}} = 1/C_{\mathrm{TE}}$, and $\eta_0 = (\mu_0\varepsilon_0)^{1/2}$. If C_{TE} and C_{TM} are represented generically as C and the z-directed fields E_z and H_z are represented generically as U; the solution for both TM and TE cases takes the form

$$U = -\frac{j}{8}\sum_{n=-\infty}^{\infty}\int_{-\infty}^{\infty} \cdot \left[H_\nu^{(1)}(kr) - \frac{H_\nu^{(1)\prime}(ka) - jCH_\nu^{(1)}(ka)}{H_\nu^{(2)\prime}(ka) - jCH_\nu^{(2)}(ka)}H_\nu^{(2)}(kr)\right] \cdot H_\nu^{(2)}(kr_1)\exp[j\nu(\phi - \phi_1) - 2jn\nu\pi]\,d\nu \tag{2}$$

where (r_1, ϕ_1) and (r, ϕ), respectively, describe the line source location and observation point as shown in Fig. 1. In the shadow region, the integral (2) can be evaluated in terms of a residue series. Substitution of $C_{\rm TE}$ and $C_{\rm TM}$ for C determines whether (2) is an expression for the z component of the magnetic or electric field. The normalization is the same as in [10] and $r_1 > r$ has been assumed.

A. Formulation for the Deep-Shadow Region

For an observation point in the shadow region, the dominant diffracted-ray contributions (i.e., those that do not involve multiple encirclements of the cylinder) derive from the $n = 0$ and $n = 1$ terms in the summation and are associated with the second term within the integrand. Let U_d represent the contribution from a single such diffracted ray. In precise analogy with [10], an approximation for U_d is derivable from (2) in the asymptotic frequency regime in the form

$$U_d = \frac{m \exp[-jk(s_1 + s_2 + t)]}{k\sqrt{s_1 s_2}} \times \sum_{p=1}^{\infty} \frac{q^2 e^{-j\xi\tau_p}}{(q^2 - \tau_p)[w_2'(\tau_p)]^2} e^{-j(\tau_p/2u_g)^2} \tag{3}$$

where $m = (ka/2)^{1/3}$ and τ_p is the pth root of

$$w_2'(\tau) - q w_2(\tau) = 0 \tag{4}$$

with $q = -jmC$. The functions $w_2(\tau)$ and $w_2'(\tau)$ are the well-known Fock-type Airy function and its derivative. The parameters t and ξ in (3) are used to represent, respectively, the quantities $a\theta$ and $m\theta$ where

$$\theta = -\left[\cos^{-1}\left(\frac{a}{r_1}\right) + \cos^{-1}\left(\frac{a}{r}\right) + \alpha\right]. \tag{5}$$

The angle α is either $-(\phi - \phi_1)$ for a diffracted ray traveling counterclockwise in Fig. 1 or $\phi - \phi_1 - 2\pi$ for a diffracted ray traveling clockwise in Fig. 1. The parameters s_1 and s_2 are associated in the usual way [1] with the path of the diffracted ray and are given by $s_1 = (r_1^2 - a^2)^{1/2}$ and $s_2 = (r^2 - a^2)^{1/2}$ while u_g is given by

$$u_g = \frac{1}{m}\left(\frac{k s_1 s_2}{2(s_1 + s_2)}\right)^{1/2}. \tag{6}$$

The parameter u_g, defined by (6) and represented simply as u in [10], is subscripted here in order to indicate that a geometrical value, i.e., the right-hand side of (6) for a specific problem geometry, is being represented.

Since (3) can be understood as the impedance-boundary analog of the solution given in [10] for the conducting case, the geometrical interpretation of (3) in a GTD context is straightforward. In particular, attenuation constants and diffraction coefficients appropriate to a Keller-type modal representation of the field [5] can be obtained for the impedance cylinder from (3). This construction will provide, as discussed in [10], a uniform GTD representation for the field in the shadow region. The attenuation constants take the form

$$\alpha_p = j\frac{m}{a}\tau_p \tag{7}$$

while the diffraction coefficients are given by

$$D_p(Q_{1,2}) = \left[\sqrt{\frac{2\pi}{k}}\frac{2q^2 m e^{j\pi/4}}{(q^2 - \tau_p)[w_2'(\tau_p)]^2}\right]^{1/2} \exp\left(\frac{-jm^2\tau_p^2}{2ks_{1,2}}\right). \tag{8}$$

Q_1 and Q_2 represent the diffracted-ray attachment and detachment points in accordance with the GTD-ray formalism. The presence within each modal diffraction coefficient given by (8) of an exponential factor involving τ_p^2 causes the modal series representation defined by (7) and (8) to maintain convergence at the shadow boundary and as the lit region ($\xi < 0$) is entered. This is a feature not observed in Keller's original formulation.

While (3) or, equivalently, (7) and (8) provide a valid representation as $\xi \to 0$, application of the solution in this form will, for the purposes of this paper, be strictly limited so as to exclude the vicinity of the shadow boundary. As has been noted (and is described in detail in [10]), when these formulas are employed at the shadow boundary, many terms are required to achieve residue-series convergence whenever u_g is greatly in excess of unity. Computation of the fields in the transition region with the aid of a limited number of identified pole locations will be achieved instead via the new procedure based on the function $p^*(\xi, q, u)$, which is shortly to be introduced. In Section IV, a scheme for computing the entire scattered field from ten residue-series terms plus GO will be described and (3) or (7) and (8) will be seen to play a role only for ξ somewhat larger than zero. Finally, it should be noted that the pole locations in question are the roots of (4) that have received extensive discussion [12] and can be calculated quite generally using a fourth-order Runge–Kutta formula [13].

B. Formulation for the Transition Region

1) Shadow-Transition Region: According to [1], the field associated with a single diffracted ray in the shadow region of an impedance cylinder is represented in UTD format as

$$U_d = \frac{jm}{2\sqrt{\pi}}\frac{e^{jk(s_1+s_2+t)}}{k\sqrt{s_1 s_2}}\left[\frac{-F(X)}{2\sqrt{\pi}\xi} + p^*(\xi, q)\right] \tag{9}$$

where $X = (u_g\xi)^2$. The function $F(X)$ is defined in terms of a Fresnel integral [4]; $p^*(\xi, q)$ is a Pekeris function given by

$$p^*(\xi, q) = \frac{1}{2\sqrt{\pi}\xi} + \frac{1}{\sqrt{\pi}}\int_{-\infty}^{\infty} \frac{V'(\tau) - qV(\tau)}{w_2'(\tau) - q w_2(\tau)} e^{-j\xi\tau}\, d\tau \tag{10}$$

and $2jV(\tau) = w_1(\tau) - w_2(\tau)$. Observe now that in the most straightforward way, (3) can be rewritten in the form of (9) provided only that $p^*(\xi, q)$ is replaced by

$$p^*(\xi, q, u) = \frac{F[(u\xi)^2]}{2\sqrt{\pi}\xi} - 2j\sqrt{\pi}\sum_{p=1}^{\infty} \frac{q^2 e^{-j\xi\tau_p} e^{-j(\tau_p/2u)^2}}{(q^2 - \tau_p)[w_2'(\tau_p)]^2} \tag{11}$$

with the understanding that the argument u is to be assigned the value of u_g from (6).

Because (3) and (9) can both be expected to accurately represent the transition-region fields, it may be surmised that $p^*(\xi, q, u_g)$ and $p^*(\xi, q)$ are nearly equivalent functions. It is this surmise that forms the basis for the new approach to computing the transition-region fields. A key ingredient is that inasmuch as this approximate equivalence can be expected to hold for a wide range of u_g values, it may therefore be presumed that the u dependence of $p^*(\xi, q, u)$ is weak.

The above statements can be made more precise by taking advantage of certain results from [10], which treats the case of perfect conductivity. In the limiting cases $q = 0$ and $q \to \infty$, the function $p^*(\xi, q)$ reduces to the more familiar UTD functions $p^*(\xi)$ and $q^*(\xi)$ [4] while, according to the above argument, $p^*(\xi, q, u)$ provides approximate equivalents expressed in terms of familiar roots and turning values of the Airy function and its derivative [7]. With these limiting correspondences in mind, it is possible to readily understand both functions $p^*(\xi, q)$ and $p^*(\xi, q, u)$ as arising from the same integral, which is a generalization of [10, eq. (7c)] to cases other than $q = 0$ and $q \to \infty$. The generalization in question is obtained from [10, eq. (7c)] by replacing each Airy function ratio with the more general form of Airy function ratio that appears within the integral in (10). Also, it is to be understood that in [10, eq. (7c)], the formal arguments ξ and u have been evaluated at $m\theta$ and u_g, respectively. According to results provided in [10], either $p^*(\xi, q)$ or $p^*(\xi, q, u)$ is obtained from the one integral, depending on whether the τ^2 term that appears in the argument of the exponentials is, respectively, ignored or retained. Note that the coefficient of the τ^2 term in [10, eq. (7c)] may be identified as $-j/(2u)^2$. It follows that for arbitrary positive ξ, $p^*(\xi, q, u)$ approaches $p^*(\xi, q)$ as u becomes large, as may be explicitly verified via residue-series evaluation of the integral in (10). For values of u_g such that (3) and (9) can both be expected to provide an accurate representation of the shadow-region fields, it may be concluded that convergence of $p^*(\xi, q, u)$ to $p^*(\xi, q)$ has nearly been achieved.

Numerical data provided in [10] for a perfectly conducting cylinder, both in the case of TE fields (i.e., $q = 0$) and in the case of TM fields (i.e., $q \to \infty$) indicate that shadow-boundary field values predicted by (3) and (9) are nearly identical for u_g greater than unity. Convergence of $p^*(\xi, q, u)$ to $p^*(\xi, q)$ should, therefore, be understood as occurring rapidly for $\xi = 0$ as u increases beyond unity. In the regime $u_g \geq 1.0$, therefore, it should not matter whether $p^*(\xi, q)$ is employed in (9) or whether $p^*(\xi, q)$ is replaced by $p^*(\xi, q, u)$ with u given by u_g in (6) or, more importantly, with u arbitrarily assigned any other value within the convergence region. The number of residue-series terms required to evaluate $p^*(\xi, q, u)$ via (11) increases dramatically with u, but if u is chosen close to unity, only a modest number of terms will be required. In other words, it should be possible to accurately and efficiently compute the fields in the shadow transition region using $p^*(\xi, q, u)$ in (9) with a value of u chosen close to unity for rapid convergence. It is important to reemphasize that (9) with $p^*(\xi, q, u)$ in place of $p^*(\xi, q)$ is really the same as (3), except for the exploitation of the weak u dependence for convergence purposes.

2) Lit-Transition Region: Since the Fresnel-integral term and the residue-series term that add to give $p^*(\xi, q, u)$ in (11) are individually well behaved as $\xi \to 0$, it may be anticipated that $p^*(\xi, q, u)$ can be extended to the lit region and employed to construct a representation of the lit-region fields. In the absence of any formal lit-region solution involving $p^*(\xi, q, u)$, the straightforward approach is to employ $p^*(\xi, q, u)$ as an approximation for $p^*(\xi, q)$, just as in the shadow transition region. Though the foregoing discussion implies that such an approximation will be accurate at $\xi = 0$, there is no reason to believe that this approximation will maintain accuracy far into the lit region. The fundamental question is whether accuracy is maintained through enough of the lit transition region that a representation for the entire lit region can be defined with the aid of GO.

The extension of $p^*(\xi, q, u)$ into the lit region is not given by (11), but requires the inclusion of an additional term in order to preserve continuity. For $\xi < 0$, the definition

$$p^*(\xi, q, u) = \frac{F[(u\xi)^2]}{2\sqrt{\pi}\xi} + ue^{j[\pi/4+(u\xi)^2]} - 2j\sqrt{\pi}\sum_{p=1}^{\infty} \frac{q^2 e^{-j\xi\tau_p} e^{-j(\tau_p/2u)^2}}{(q^2 - \tau_p)[w_2'(\tau_p)]^2} \tag{12}$$

may be regarded as unique because the small argument expansion (in powers of $u\xi$ as $\xi \to 0_-$) for the sum of the first two terms in (12) is identical to the small argument expansion (as $\xi \to 0_+$) [6] for the Fresnel integral term in (11).

Use of the UTD representation in the lit-transition region requires consideration of direct- and reflected-ray contributions. The reflected-ray contribution is determined by the UTD reflection coefficient given for angle of incidence θ_i by

$$R_{\mathrm{UTD}}(\xi)' = -\sqrt{\frac{-4}{\xi'}} e^{-j[\pi/4+(\xi')^3/12]} \times \left[\frac{-F(kL'\tilde{a}')}{2\sqrt{\pi}\xi'} + p^*(\xi', q)\right] \tag{13}$$

where $\xi' = -2m\cos\theta_i$, $\tilde{a}' = 2\cos^2\theta_i$, $L' = s_1's_2'/(s_1' + s_2')$, and s_1' and s_2' are the distances, respectively, from the line source to the point of reflection and from the point of reflection to the observation point. In the vicinity of the shadow boundary, $p^*(\xi', q, u)$ with u close to unity can be expected to accurately approximate $p^*(\xi', q)$ in (13) and can readily be evaluated from a modest number of residue-series terms. As ξ' becomes more negative, however, the residue series in (12) becomes more slowly convergent. As will be seen in Section IV, the approach of $p^*(\xi', q, u)$ to $p^*(\xi', q)$ with increasing u also occurs more slowly. While (12) can, therefore, be expected to be useful only in a portion of the lit region, it will be demonstrated in Section IV that a complete representation is available via a transition to GO.

III. Coated Cylinder

The geometry for a line source in the presence of a coated cylinder is shown in Fig. 2. The interior cylinder of radius a is assumed to be perfectly conducting, while the constitutive parameters of the coating are designated as ϵ_c and μ_c. Boundary

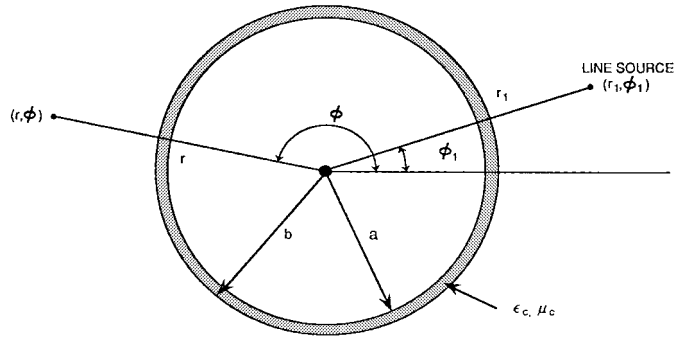

Fig. 2. Geometry for the line-source and coated-cylinder problem.

conditions appropriate to the geometry of Fig. 2 include zero tangential electric field at the surface $r = a$ and continuity of tangential electric and magnetic fields at $r = b$. Let the z-directed electric field in the case of an electric line source (the TM case) and the z-directed magnetic field in the case of a magnetic line source (the TE case) be denoted generically as U. The solution for U is once again represented by (2) except that the constant C becomes replaced by a ν-dependent function given by

$$C_\nu^{\mathrm{TM}} = -j\frac{k_c\mu_0}{k\mu_c}\frac{J_\nu(k_ca)N_\nu'(k_cb) - N_\nu(k_ca)J_\nu'(k_cb)}{J_\nu(k_ca)N_\nu(k_cb) - N_\nu(k_ca)J_\nu(k_cb)} \quad (14a)$$

for the TM case and by

$$C_\nu^{\mathrm{TE}} = -j\frac{k_c\epsilon_0}{k\epsilon_c}\frac{J_\nu'(k_ca)N_\nu'(k_cb) - N_\nu'(k_ca)J_\nu'(k_cb)}{J_\nu'(k_ca)N_\nu(k_cb) - N_\nu'(k_ca)J_\nu(k_cb)} \quad (14b)$$

for the TE case, where $k_c = \omega\sqrt{\mu_c\epsilon_c}$.

A. Formulation for the Deep-Shadow Region

In order to obtain coated-cylinder equivalents to the impedance-cylinder expressions in Section II, it is once again required to express U in a residue-series format. In particular, let us consider the dominant contributions to the field from the nonencircling diffracted rays. Such contributions can be approximated as

$$U_d = \frac{j}{2}k\sum_{p=1}^{\infty}\frac{1}{\sqrt{r_1\sin\beta_{1p}}\sqrt{r\sin\beta_{2p}}}\frac{b(\nu_p)}{\frac{\partial}{\partial\nu}d(\nu)|_{\nu_p}} \cdot \exp[-j(kr_1\sin\beta_{1p} - \nu_p\beta_{1p} + kr\sin\beta_{2p} - \nu_p\beta_{2p} - \nu_p\alpha)] \quad (15)$$

where

$$b(\nu) = H_\nu^{(1)'}(kb) - jC_\nu H_\nu^{(1)}(kb) \quad (16a)$$

and

$$d(\nu) = H_\nu^{(2)'}(kb) - jC_\nu H_\nu^{(2)}(kb) \quad (16b)$$

and where $\alpha = -(\phi - \phi_1)$ for a counterclockwise traveling ray corresponding to $n = 0$ in (2), while $\alpha = \phi - \phi_1 - 2\pi$ for a clockwise traveling ray corresponding to $n = 1$ in (2). The pole locations ν_p are defined by $d(\nu_p) = 0$. The Debye approximation has been used in (15) for Hankel functions of argument kr_1 and kr under the assumption that the source and observation point are not close to the cylinder surface. Also, β_{1p} and β_{2p} are given by

$$\beta_{ip} = \cos^{-1}\left(\frac{\nu_p}{kr(i)}\right) \quad (17)$$

where $r(1) = r_1$ and $r(2) = r$.

In [2], certain approximations are introduced to transform (15) into a more convenient form and a GTD ray interpretation is then provided. Note that the GTD ray paths, which thereby arise, are those employed in [1], [4], and also in Section II and should be distinguished from the ray paths that occur within the coated-cylinder formulation described in [14]. The approximations in [2] cause the resulting solution to lose convergence in the vicinity of the shadow boundary and a heuristic method for transition-integral evaluation is introduced to obtain the correct behavior at small ξ. Here, the first requirement is for a residue-series expression that corresponds to (3) for the impedance cylinder. Such an expression can be obtained from (15) by approximating the argument of the exponential term more precisely than is done in [2]. With $m = (kb/2)^{1/3}$, let τ_p be defined as $(\nu_p - kb)/m$ and expand the exponentiated term in (15) in powers of τ_p through order τ_p^2. The expansion is given by

$$kr(i)\sin\beta_{ip} - \nu_p\beta_{ip} \approx ks_i - \nu_p\cos^{-1}\left(\frac{b}{r(i)}\right) + \frac{m^2\tau_p^2}{2ks_i} \quad (18)$$

where $s_1 = (r_1^2 - b^2)^{1/2}$ and $s_2 = (r^2 - b^2)^{1/2}$. When this approximation is inserted into (15), the resulting expression for the field contribution due to a single diffracted ray becomes

$$U_d = -\frac{2}{k\sqrt{s_1s_2}}\sum_{p=1}^{\infty} \times \frac{e^{-j\nu_p\theta}\cdot e^{-j(\tau_p/2u_g)^2}}{\pi kbH_{\nu_p}^{(2)}(kb)\frac{\partial}{\partial\nu}d(\nu)\big|_{\nu_p}}\cdot e^{-jks_1}\cdot e^{-jks_2} \quad (19)$$

where θ is given by (5) with $a \to b$ and where the inverse factors of $(r_1\sin\beta_{1p})^{1/2}$ and $(r\sin\beta_{2p})^{1/2}$ inside of the summation in (15) have been approximated as $s_1^{1/2}$ and $s_2^{1/2}$, respectively. The parameter u_g has the usual meaning given by (6).

A GTD interpretation of an expression identical to (19), but without the exponential factors involving u_g, is provided in [2] while the geometrical interpretation of these factors is apparent from [10]. The attenuation constants appropriate to a modal series representation based on (19) are defined by (7) with $a \to b$ and with τ_p given by $(\nu_p - kb)/m$. The modal diffraction coefficients are given by

$$D_p(Q_{1,2}) = \left[\sqrt{\frac{2}{\pi k}}\frac{4}{kb}\frac{e^{-j3\pi/4}}{H_{\nu_p}^{(2)}(kb)\frac{\partial}{\partial\nu}d(\nu)\big|_{\nu_p}}\right]^{1/2} \cdot \exp\left(\frac{-jm^2\tau_\rho^2}{2ks_{1,2}}\right) \quad (20)$$

and differ from those in [2] only by virtue of the new exponential factors, which, as before, provide for convergence in the shadow-boundary transition region.

B. Formulation for the Transition Region

While (19) can be expected to remain accurate throughout the shadow region, computation of transition-region fields via (19) will not, in general, be efficient inasmuch as large numbers of residue-series terms may be required. This possibility was previously discussed in connection with (3) for the impedance-cylinder case. This difficulty can, once again, be overcome via a transformation into the UTD format given by (9). Recasting (19) into the form of (9) (for $\xi > 0$) and subsequent analytic continuation (for $\xi < 0$) leads to the definition of a function $p^*(\xi, q, u)$ applicable to coated-cylinder problems as

$$p^*(\xi,q,u) = \frac{F[(u\xi)^2]}{2\sqrt{\pi}\xi} + \sum_{p=1}^{\infty} \frac{4je^{-jm\theta\tau_p}e^{-j(\tau_p/2u)^2}}{\sqrt{\pi}mkbH_{\nu_p}^{(2)}(kb)\frac{\partial}{\partial\nu}\,d(\nu)\big|_{\nu_p}} \qquad (\xi > 0) \quad (21a)$$

and

$$p^*(\xi,q,u) = \frac{F[(u\xi)^2]}{2\sqrt{\pi}\xi} + ue^{j[\pi/4+(u\xi)^2]} + \sum_{p=1}^{\infty} \frac{4je^{-jm\theta\tau_p}e^{-j(\tau_p/2u)^2}}{\sqrt{\pi}mkbH_{\nu_p}^{(2)}(kb)\frac{\partial}{\partial\nu}\,d(\nu)\big|_{\nu_p}} \qquad (\xi < 0) \quad (21b)$$

where the dependence on such parameters as the coating thickness, dielectric constant, etc. is understood. Representing the field in the shadow-transition region of a coated cylinder by (9) with $p^*(\xi, q)$ replaced by $p^*(\xi, q, u)$ for $u = u_g$ is equivalent to using (19). It may be anticipated that for u larger than unity $p^*(\xi, q, u)$ defined by (21a) and (21b) will asymptotically approach a coated cylinder Pekeris integral $p^*(\xi, q)$ such as is defined in [2]. Because of the slowness of the expected u variation, it should be possible to compute the transition-region fields via the UTD expressions (9) and (13) with $p^*(\xi, q)$ replaced by $p^*(\xi, q, u)$ from (21a) and (21b) and u chosen close to unity for rapid-series convergence.

It is interesting to compare the current treatment of coated cylinder transition-region fields with previous treatments. In [2], it is proposed that the coated-cylinder transition integral can be approximated by an impedance cylinder Pekeris integral computed for a value of q determined by the $p = 1$ modal impedance. The latter Pekeris integral is to be evaluated by the heuristic method described in [1] and [2]. In [3] the Pekeris integral defined for the generalized IBC case is evaluated by direct numerical integration. In contrast, computation of coated-cylinder transition-region fields via (21a) and (21b) does not require recourse to any approximate boundary condition. By way of comparison with the formulation described in Section II, however, it must be noted that the zeroes of (16b) are not so easily obtained as the roots of (4). Applicable methods include the contour-integral search technique of Singaraju *et al*. [15] and Davidenko's method [16].

IV. Numerical Results

In Sections II and III, formulations are proposed as permitting the fields in the deep shadow and transition regions of an impedance or coated cylinder to be accurately determined from knowledge of a limited number of pole locations. In the transition region, the formulations that have been described involve the function $p^*(\xi, q, u)$ introduced in this paper, while in the deep-shadow region, the formulations are simple extensions of [10]. Here it will be numerically demonstrated that these formulations do indeed possess the features ascribed to them and that together with the GO solution for the deep-lit-region fields, they can be used to compute the entire field scattered by an impedance or coated-cylinder with the aid of limited pole-location data. Toward this end, it will be necessary to organize the various formulations (including GO) by defining a range of applicability for each. In other words, for the purposes of this paper, the terms "deep-lit region," "deep-shadow region," and "transition region" must be given precise definitions in terms of ξ regions over which the corresponding formulas from either Sections II, III, or GO can be effectively applied. Furthermore, the transition-region formulas described in Sections II and III rely upon the function $p^*(\xi, q, u)$ computed for an advantageous u value that will, in general, be different from u_g in (6). It will be necessary to identify an optimal value for the selectable parameter u in such a way that $p^*(\xi, q, u)$ can effectively be employed as an approximation for $p^*(\xi, q)$ within the UTD transition-region formulas. It was decided, with a certain degree of arbitrariness, that evaluation of the various formulas should be limited to require no more than ten residue-series terms. Selection of the ξ-regions over which the different formulas are taken to apply, as well as of the optimal u value, will be based on this requirement.

As a first step, it will be necessary to assess the behavior of $p^*(\xi, q, u)$ both with respect to the rapidity with which $p^*(\xi, q)$ is approached as u increases and also with respect to the number of residue-series terms required for accurate evaluation at given values of u and ξ. It is especially important to recall at this point the fact that the argument for the near equivalence of $p^*(\xi, q)$ and $p^*(\xi, q, u)$ for u near unity was developed for the shadow transition region only. A slower approach of $p^*(\xi, q, u)$ to $p^*(\xi, q)$ may be anticipated at increasingly negative values of ξ. It will be seen that effective use of $p^*(\xi, q, u)$ at large negative ξ is not possible and it is for this reason that a crossover to the GO representation needs to be forcibly imposed as ξ decreases. Identification of criteria for switching among the formulas as well of the optimal u value will be based on the numerical examination of $p^*(\xi, q, u)$. In the end, it will be shown that it is possible both to achieve a smooth transition among expressions suitable in different ξ regions and to obtain results in close agreement with results obtained via eigenfunction series methods.

A. $p^*(\xi, q, u)$ Versus $p^*(\xi, q)$

While comparisons between $p^*(\xi, q, u)$ and $p^*(\xi, q,)$ were made in both the impedance- and coated-cylinder cases, a comprehensive analysis of the asymptotic approach of $p^*(\xi, q, u)$ to $p^*(\xi, q)$ was carried out only for the case where these functions are defined by (11), (12), and (9), respectively.

The justification for applying the conclusions derived from this analysis to the coated-cylinder case was based on the observation that accurate scattered-field values and smooth ξ-region transitions were thereby obtained. Computation of $p^*(\xi, q, u)$ via (11) or (12) was based on roots of (4) calculated by the method described by Hill and Wait [13]. Implementation of a capability to calculate up to 50 of these roots made evaluation of $p^*(\xi, q, u)$ possible over a large range of u and ξ values. Fig. 3(a) and (b) compares, respectively, the real and imaginary parts of $p^*(\xi, q, u)$ for $u = 1.0$, $u = 1.25$, and $u = 2.0$ with the real and imaginary parts of $p^*(\xi, q)$ computed via Pearson's numerical integration technique [9]. Three values of q, specifically $q = 0$, $q \to \infty$, and $q = 1.0e^{-j\pi/4}$ are represented. For $q = 0$ and $q \to \infty$, the familiar UTD function $p^*(\xi)$ or $q^*(\xi)$, as appropriate, should be understood in place of $p^*(\xi, q)$. The convergence of $p^*(\xi, q, u)$ to $p^*(\xi, q)$ is readily apparent from the quality of agreement between the $u = 2.0$ and the $p^*(\xi, q)$ curves over the range of ξ values depicted. In contrast, the $u = 1.0$ curves show agreement with the $p^*(\xi, q)$ curves provided that $\xi \geq -1.0$ but begin to diverge from $p^*(\xi, q)$ at smaller ξ values. Essentially identical results were observed in comparisons of $p^*(\xi, q, u)$ and $p^*(\xi, q)$ for the real q cases considered in [1].

Fig. 3(a) and (b) confirms the expectation that for u close to unity, $p^*(\xi, q, u)$ should closely approximate $p^*(\xi, q)$ in the vicinity of $\xi = 0$ and confirms, as well, the further expectation that the asymptotic approach of $p^*(\xi, q, u)$ to $p^*(\xi, q)$ will occur more slowly as ξ becomes large and negative. The choice $u = 2.0$ appears to provide for close agreement between $p^*(\xi, q, u)$ and $p^*(\xi, q)$ throughout the region $-2.0 < \xi < 2.0$. Unfortunately, this choice is unsatisfactory in terms of limiting the number of pole locations required to evaluate $p^*(\xi, q, u)$ via (12). This is illustrated in Table I, which gives, for certain values of u and ξ, the number of residue-series terms required in (11) or (12) to ensure that $p^*(\xi, q, u)$ is determined to within 5×10^{-3} absolute error in both the real and imaginary part. It is clear from Table I that for $\xi < -1.5$, evaluation of $p^*(\xi, q, u)$ from ten or fewer pole locations requires that u be chosen very near to unity. Since for u near unity $p^*(\xi, q, u)$ is diverging from $p^*(\xi, q)$ in the vicinity of $\xi = -2.0$, obtaining a complete solution that relies on ten or fewer residue-series terms was determined to be possible only if the GO representation could be employed at values of ξ somewhat larger than -2.0.

Parenthetically, it may be noted that inasmuch as direct application of (3) requires the same residue series as $p^*(\xi, q, u)$ except that u must be evaluated as u_g from (6), Table I should be understood as providing an illustration of the convergence difficulties that the new procedure avoids. In particular, for $\xi \leq 0$, when u_g is increased arbitrarily beyond the u range of Table I, the number of residue-series terms required will continue to increase without limit.

B. ξ-Region Breakdown and Optimal u

To attempt to identify criteria for switching from the $p^*(\xi, q, u)$ representation to GO in the lit region as ξ becomes large and negative, it was necessary to examine the behavior

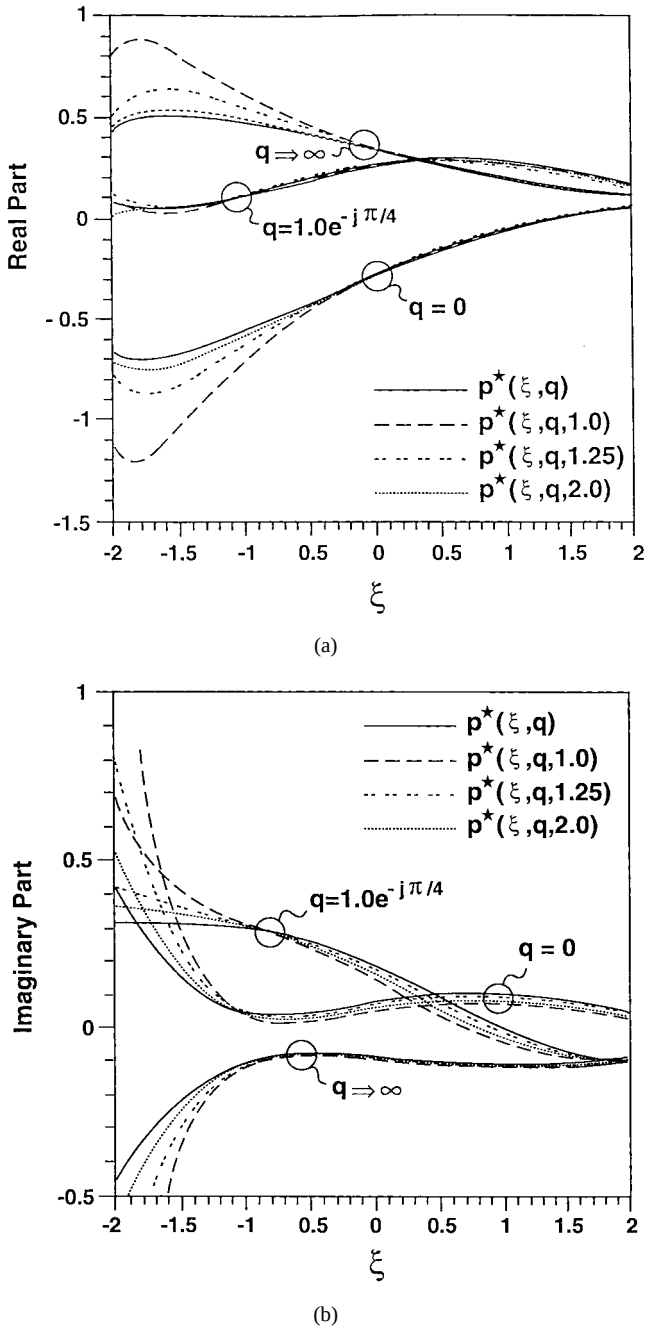

Fig. 3. (a) The real part of $e^{-j\pi/4}p^*(\xi, q)$ versus the real part of $e^{-j\pi/4}p^*(\xi, q, u)$ for $u = 1.0,\ 1.25$, and 2.0. (b) The imaginary part of $e^{-j\pi/4}p^*(\xi, q)$ versus the imaginary part of $e^{-j\pi/4}p^*(\xi, q, u)$ for $u = 1.0,\ 1.25$, and 2.0.

of the reflection coefficient computed from $p^*(\xi, q, u)$, as well as the behavior of the GO reflection coefficient given by

$$R_{\mathrm{GO}}(\theta_i) = -\frac{C - \cos(\theta_i)}{C + \cos(\theta_i)} \tag{22}$$

in the region $-2.0 \leq \xi \leq -1.0$ where, for moderate values of u, $p^*(\xi, q, u)$ begins to diverge from $p^*(\xi, q)$. For evaluation purposes, the standard UTD representation was used to provide reflection-coefficient values that could be expected to be accurate throughout the lit region. A comparison of reflection

TABLE I
NUMBER OF TERMS REQUIRED FOR EVALUATION OF $p^*(\xi, q, u)$ VIA (11) or (12)

u \ξ	+0.5	0.0	-0.5	-1.0	-1.5	-2.0
1.00	2	2	3	4	5	7
1.25	2	3	4	6	9	12
1.50	3	4	6	9	14	19
2.00	3	6	11	19	29	42

coefficients computed from (22) and via UTD with $p^*(\xi, q)$ obtained from data in [1] and from numerical integration (as in [9]) appeared to indicate that $R_{\rm GO}$ begins to lose accuracy slowly as ξ increases above -2.0. The reflection coefficient as computed from $p^*(\xi, q, u)$ via (13) was determined to be accurate when ξ is larger than -2.0 provided that u is chosen as large as 2.0. As noted above, for $\xi < -1.5$, the requirement that $p^*(\xi, q, u)$ be evaluated from ten or fewer residue-series terms forbids such a choice. On the other hand, as is especially clear in Fig. 4(b), the choice $u = 1.0$ causes $p^*(\xi, q)$ to be poorly approximated by $p^*(\xi, q, u)$ for $\xi < 1.5$. A compromise value of u was, therefore, determined to be required and the value $u = 1.25$, suggested by the data in Table I, was adopted after some experimentation. An important motivation for this choice was derived from the observation that a smooth transition between $R_{\rm GO}$ and $R_{\rm UTD}$ computed from $p^*(\xi, q, 1.25)$ could be effected by means of a simple linear interpolation scheme. In this scheme, $R_{\rm GO}$ is recovered as ξ is decreased below -1.8, while at $\xi = -1.3$ and above, the reflection coefficient may be identified with $R_{\rm UTD}$ as obtained from (13) with $p^*(\xi, q, 1.25)$ in place of $p^*(\xi, q)$.

Amplitudes and phases of reflection coefficients computed by various methods for $q = 0.5e^{-j\pi/4}$ and a representative geometry are shown in Fig. 4(a) and (b). As expected, when $R_{\rm UTD}(\xi)$ is computed using values of $p^*(\xi, q)$ obtained from numerical integration, close agreement is observed between $R_{\rm UTD}$ and $R_{\rm GO}$ at large negative ξ. On the other hand, for small negative ξ, it does not seem to matter whether $p^*(\xi, q)$ or $p^*(\xi, q, u = 1.25)$ is employed to compute $R_{\rm UTD}$. What is important to observe in these figures is that centered at approximately $\xi = -1.5$, there is a region in which neither $R_{\rm GO}$ nor $R_{\rm UTD}$ computed from $p^*(\xi, q, u = 1.25)$ has deviated markedly from the correct behavior, which may be identified with $R_{\rm UTD}$ computed from $p^*(\xi, q)$. The reflection coefficient R_I obtained via the interpolation procedure can, therefore, be expected to provide an acceptable approximation. The availability of this interpolation procedure dictated the selection of $u = 1.25$ as an "optimal" value for the parameter u. While a larger value could, of course, be used at added computational expense (because the number of residue-series terms required to achieve convergence in (12) would increase), numerical investigations revealed that some loss in accuracy would result from allowing u to be as small as 1.0.

For convenience, Table II summarizes the foregoing discussion by listing the various formulas that have been described together with the ξ regions to which these formulas can be taken to apply. Observe that the ξ-region boundaries

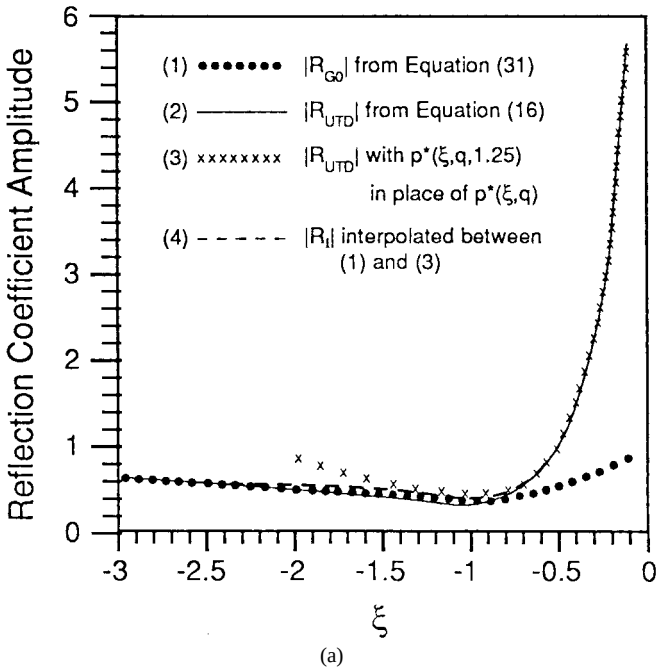

Fig. 4. (a) Amplitude of the reflection coefficient computed by various means for plane wave incidence on a cylinder of radius $a = 10\lambda$. Other parameters are $q = 0.5e^{-j\pi/4}$ and $u_g = 2.0$. (b) Phase of the reflection coefficient computed by various means for plane wave incidence on a cylinder of radius $a = 10\lambda$. Other parameters are $q = 0.5e^{-j\pi/4}$ and $u_g = 2.0$.

and optimal u value for the coated cylinder were simply adopted from the impedance cylinder analysis. For coated-

TABLE II
ξ-REGION BREAKDOWN CORRESPONDING TO $p^*(\xi, q, u = 1.25)$ COMPUTED FROM TEN TERMS

	Region I $\xi \le -1.8$	Region II $-1.8 \le \xi \le -1.3$	Region III $-1.3 \le \xi \le 0.0$	Region IV $0.0 \le \xi \le 0.5$	Region V $\xi \ge 0.5$
Impedance cylinder (Section II)	Reflected-ray term based on GO reflection coefficient (22)	Reflection coefficient is an interpolation between I & III formulas	UTD reflection coefficient (13) but $p^*(\xi,q,u)$ in (12) replaces $p^*(\xi,q)$	Diffracted-ray term (9) from UTD; $p^*(\xi,q,u)$ in (11) replaces $p^*(\xi,q)$	Diffracted-ray term from (3) or via Keller modes using (7) and (8)
Coated cylinder (Section III)	Reflected-ray term based on GO reflection coefficients (23a) and (23b)	Reflection coefficient is an interpolation between I & III formulas	UTD reflection coefficient (13) but $p^*(\xi,q,u)$ in (21b) replaces $p^*(\xi,q)$	Diffracted-ray term (9) from UTD; $p^*(\xi,q,u)$ in (21a) replaces $p^*(\xi,q)$	Diffracted-ray term from (19) or via Keller modes using (7) and (20)

cylinder problems, (21a) and (21b) rather than (11) and (12) are employed to define $p^*(\xi, q, u)$, while the GO reflection coefficient is given by

$$R_{\mathrm{GO}} = -\frac{\eta_0 \cos\theta_t - j\eta_c \cos\theta_i \tan(k_c d \cos\theta_t)}{\eta_0 \cos\theta_t + j\eta_c \cos\theta_i \tan(k_c d \cos\theta_t)} \text{ (TM case)} \tag{23a}$$

and

$$R_{\mathrm{GO}} = \frac{\eta_0 \cos\theta_i - j\eta_c \cos\theta_t \tan(k_c d \cos\theta_t)}{\eta_0 \cos\theta_i + j\eta_c \cos\theta_t \tan(k_c d \cos\theta_t)} \text{ (TE case)} \tag{23b}$$

where $d = b - a, \eta_c = \sqrt{\mu_c/\epsilon_c}$, and

$$\cos\theta_t = \sqrt{1 - \left(\frac{k_0}{k_c}\sin\theta_i\right)^2}. \tag{24}$$

Finally, note that while discussion has focused on the problematic lit region, formula switching in Table II is also defined to occur at the shadow boundary and at $\xi = +0.5$. The formula crossover at $\xi = 0$ is between the lit- and shadow-region representations of $p^*(\xi, q, u)$. The crossover at $\xi = +0.5$ is between the transition and deep-shadow representations from Sections II and III. In the shadow region, $p^*(\xi, q, u)$ is employed within (9), the use of which, at arbitrarily large ξ, can lead to certain problems as is described in [10]. The deep-shadow-region representations defined in Sections II and III avoid these problems in exactly the manner described in [10]. Numerical experimentation revealed that at most eight terms will ever be required to converge (3) or (19) for $\xi \ge 0.5$, even in the limit $u_g \to \infty$. Use of the deep-shadow formulas (3) and (19) for $\xi \ge 0.5$ is, therefore, consistent with the ten-term limit that is desired for the Table II representation. As ξ is decreased below 0.5, however, these formulas may require more than ten terms if u_g large. For example, in the $u_g \to \infty$ limit, (3) becomes Keller's solution as the exponential factors $\exp(-j(\tau_p/2u_g)^2)$ go to unity. While only three terms of $p^*(\xi, q, 1.25)$ are required for convergence in the region $0.0 \le \xi \le 0.5$, the number of terms required for the Keller solution increases from eight to 26 as ξ decreases from 0.5 to 0.25 and continues to grow as the divergence at $\xi = 0$ is approached.

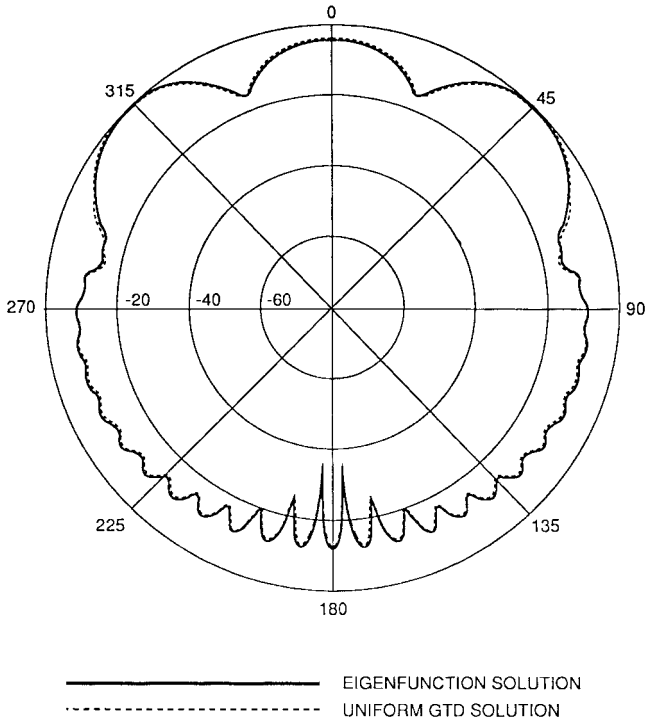

Fig. 5. Comparison of patterns obtained via the impedance-cylinder solution in Table I and via the exact solution in the vicinity of a cylinder of radius $ka = 20.0$ and relative surface impedance $C = 0.25j$. The field is evaluated at $kr = 75.0$ and is due to a line source at $kr_1 = 25.0$ and $\phi_1 = 0^\circ$.

C. Comparisons with the Exact Solution

Predictions obtained from the formulations defined by Table II were compared with corresponding eigenfunction series results for numerous cases involving both line sources and plane wave incidence. Some representative results are shown in Fig. 5 (impedance cylinder) and Fig. 6 (coated cylinder). A systematic attempt involving over 2000 separate cylinder scattering problems was made to assess the accuracy of the impedance-cylinder formulation when the amplitude of q does not exceed 100.0, while the phase of q falls in the range from 0 to $-\pi$—inclusive. Problem geometries involving values of u_g ranging from less than unity to as large as 4.0 were considered in order to demonstrate that the Table II formulations, which are based on $p^*(\xi, q, 1.25)$

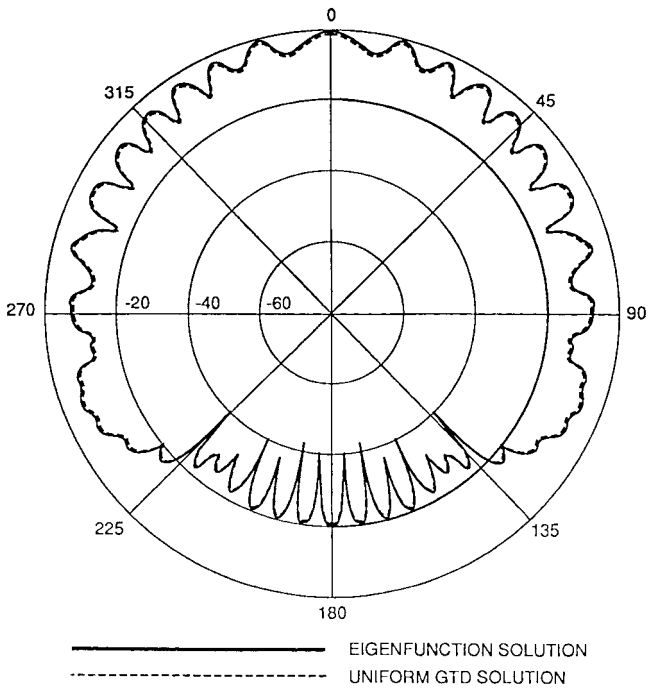

Fig. 6. Comparison of patterns obtained via the coated-cylinder solution in Table II and via the exact solution in the vicinity of a coated cylinder of outer radius $kb = 20.0$. The coating is 0.1 wavelengths thick with $\varepsilon_c = 4.0\varepsilon_0$ and $\mu_c = \mu_0$. The field is evaluated at $kr = 70.0$ and is due to a magnetic line source $kr_1 = 50.0$ and $\phi_1 = 0°$.

in the transition region, are applicable over a wide range of u_g values. While no systematic parameter-range exploration was deemed possible in the coated-cylinder case, the overall conclusion from these investigations was that accuracy on a level with that observed in Figs. 5 and 6 can quite generally be expected, except under circumstances described below.

When the phase of q is close to zero, as $|q|$ increases, the $p = 1$ root of (4) moves rapidly away from its $q = 0$ locus and may come to reside very close to the real axis. Similarly, the important zeroes of (16b), which can be found nearby to kb when $k_c d$ is small or the coating is lossy, may, under other circumstances, be found close to the real axis and far from kb. Such pole-location behavior can lead to violation of various assumptions that have been made. When a pole resides close to the real axis, inclusion of contributions from multiple encirclements is likely to be necessary. The formulations in both Sections II and III rely on the Debye approximation for Hankel functions of argument kr and kr_1. Difficulties can, therefore, be expected when an important zero [ν_p of (16b)] or when $ka + m\tau_p$ [with τ_p satisfying (4)] approaches kr or kr_1. Finally, the pole-location behavior in question can lead to a breakdown of further approximations, which are appropriate only when τ_p can be considered to be small.

While numerical investigations revealed the importance of the above considerations, particularly in the case of the Section II formulation, it was observed that upon the inclusion of multiple encirclements, accurate results were obtained from the Section III formulation in cases where dominant-mode poles resided near the real axis and far from kb. This desirable result was attributed to the slow breakdown of the approximations that lead to (19) and to the rapid growth in the denominator of (19) as a given pole is moved away from kb. Only the breakdown of the Debye approximation with the approach of a root to kr or kr_1 remained problematic. Fig. 6 was selected to demonstrate that the formulation in Section III does not lose accuracy when poles recede from kb and approach the real axis. In this example, $\nu_1 = 24.096 - j0.117$ and, it should be noted, multiple encirclements have therefore been included.

The accuracy of the Table II formulations was also observed to depend (to a certain degree) on u_g. The new formulations accurately reproduced eigenfunction series results for problems in which the condition $u_g \geq 1.25$ was satisfied. For $u_g \approx 1.25$, minor discrepancies were sometimes observed in the interpolation region $-1.8 \leq \xi \leq -1.3$. In particular, details of pattern-null behavior were not precisely reproduced when such nulls coincided with the interpolation region. In Fig. 5, the interpolation region corresponds to angular regions in the vicinity of $\phi = 70°$ and $\phi = 290°$. Note that there is some slight inaccuracy in the representation of the shallow nulls at these angular locations.

As u_g was decreased below 1.25, the breakdown of the u-invariance property began to express itself in the form of pattern irregularities, especially within the interpolation region. While the new formulations are likely to be adequate for engineering purposes for $u_g \geq 1.0$, other techniques should be employed when this condition is not satisfied. From [10], it is apparent that a large domain of practical interest is available.

Finally, some remarks should be made concerning the implementation of the various formulas. The availability of the Runge–Kutta technique permitted rapid computation of the roots of (4), especially in cases where the required τ_p could be found nearby to their $q = 0$ loci. In such cases, a ten-term evaluation of $p^*(\xi, q, 1.25)$ via (11) and (12) permitted Pekeris function values to be approximated in the interval from -2.0 to 2.0 at least five to ten times more quickly than they could be obtained via a 122-point numerical integration using the technique of [9]. (Though it should be noted that if application of the technique in [9] is restricted to $\xi \geq -2.0$, a sizable reduction in the required number of integration points is possible.) A more extensive effort was required to implement the coated-cylinder formulas. The roots of (16b) were obtained using the contour-integral search technique of Singaraju *et al.* and via the Davidenko method. Uniform asymptotic expansions [17] were used to represent Hankel functions of argument kb. Certain higher order terms were included in the representation and are described in [18]. While implementation of the coated-cylinder formulas was observed to require application of somewhat greater computational resources than were required in the impedance-cylinder case, it should be noted that these formulas allow for a very compact representation of coated-cylinder scattering problems. Once a set of pole locations has been computed by one of the standard methods noted above, arbitrary scattering problems can be easily solved via straightforward application of the Section III formulas.

V. Summary

It has been shown that a uniform GTD representation of the transition-region fields in the vicinity of an impedance or coated cylinder is available in terms of a novel function $p^*(\xi, q, u)$. By means of this function, familiar UTD transition-region formulas can be employed without recourse to numerical integration to compute values of the Pekeris integral. Instead, the required Pekeris-integral values can be approximated using $p^*(\xi, q, u)$ computed from knowledge of a limited number of pole locations.

The justification for the new procedure resides in the fact that within the transition region, $p^*(\xi, q, u)$ rapidly approaches the Pekeris function $p^*(\xi, q)$ as u is increased beyond unity. A ξ becomes more negative, however, the approach of $p^*(\xi, q, u)$ to $p^*(\xi, q)$ occurs more slowly with increasing u. Because the number of terms required for residue-series computation of $p^*(\xi, q, u)$ increases with u, it is desirable that the approximation of $p^*(\xi, q)$ via $p^*(\xi, q, u)$ occur for a value of u as close to unity as possible. On the other hand, larger values of u permit $p^*(\xi, q, u)$ to mimic the behavior of $p^*(\xi, q)$ further into the lit region. The numerical results presented in this paper were based on a ten-term computation of $p^*(\xi, q, 1.25)$. The transition region representation based on $p^*(\xi, q, 1.25)$ was smoothly joined with the GO representation of the lit-region fields and with a deep-shadow-region representation having the form of [10]. Excellent agreement with eigenfunction series results was observed over a large number of test cases.

The formulation described in Section II is very attractive from a computational perspective, because roots of (4) are readily obtained. The formulation described in Section III requires a degree of effort in order to obtain the roots of (16b), but imposes less restriction on the pole behavior.

Acknowledgment

The author would like to thank T. L. Brown of Prof. K. Naishadham of Wright State University, Dayton, OH, and Dr. R. Pogovzelski of the Jet Propulsion Laboratories, Pasadena, CA, for their fruitful discussions and the software which benefited this work. He would also like to thank P. Schaefer for her technical support.

References

[1] N. Wang and H. T. Kim, "UTD solution for the electromagnetic scattering from a circular cylinder with a constant surface impedance: Ram and inlet modeling studies—Part II," Electromagn. Sci. Lab., Dept. Elect. Eng., Ohio State Univ., Columbus, Tech. Rep. 716495-2, Contract N60530-84-C-0143 for Dept. Navy, Office Naval Weapons Ctr., China Lake, CA, Oct. 1985.

[2] H. T. Kim and N. Wang, "UTD solution for electromagnetic scattering by a circular cylinder with thin lossy coatings," *IEEE Trans. Antennas Propagat.*, vol. 37, pp. 1463–1472, Nov. 1989.

[3] H. H. Syed and J. L. Volakis, "High-frequency scattering by a smooth coated cylinder simulated with generalized impedance boundary conditions," *Radio Sci.*, vol. 26, pp. 1305–1314, Sept./Oct. 1991.

[4] P. H. Pathak, W. D. Burnside, and R. J. Marhefka, "A uniform GTD analysis of the diffraction of electromagnetic waves by a smooth convex surface," *IEEE Trans. Antennas Propagat.*, vol. AP-28, pp. 631–642, Sept. 1980.

[5] J. B. Keller, "Diffraction by a convex cylinder," *IRE Trans. Antennas Propagat.*, vol. AP-4, pp. 312–321, July 1956.

[6] R. G. Kouyoumjian and P. H. Pathak, "A uniform GTD approach to EM scattering and radiation," in *Acoustic, Electromagnetic, and Elastic Wave Scattering—Low and High Frequency Asymtotics*, V. K. Varadan and V. V. Varadan, Eds. Amsterdam, The Netherlands: North Holland, vol. II, 1986.

[7] N. A. Logan, "General research in diffraction theory," Missiles Space Div., Lockheed Aircraft Corp., 1959, vol. I, LMSD 288 087; vol. II, LMSD 288 088.

[8] J. R. Wait and M. A. Conda, "Diffraction of electromagnetic waves by smooth obstacles for grazing angles," *J. Res. Nat. Bur. Stand.*, vol. 630, pp. 181–197, Sept./Oct. 1959.

[9] L. W. Pearson, "A scheme for automatic computation of Fock-type integrals," *IEEE Trans. Antennas Propagat.*, vol. AP-35, pp. 1111–1118, Oct. 1987.

[10] P. Hussar and R. Albus, "On the asymptotic frequency behavior of uniform GTD in the shadow region of a smooth convex surface," *IEEE Trans. Antennas Propagat.*, vol. 39, pp. 1672–1680, Dec. 1991.

[11] C. Lin, W. Ni, and M. T. Yaqoob, "Direct computation of scattering in the transition region," *IEEE Antenna Propagat. Soc. Int. Symp. Dig.*, Chicago, IL, pp. 711–714, July 1992.

[12] N. A. Logan, "Numerical investigation of electromagnetic scattering and diffraction by convex objects," U.S. Air Force Geophys. Lab., Air Force Syst. Commun., Hanscom AFB, Bedford, MA, Tech. Rep. AFCRL 66-153, 1965.

[13] D. A. Hill and J. R. Wait, "Groundwave attenuation function for a spherical earth with arbitrary surface impedance," *Radio Sci.*, vol. 15, pp. 637–643, May/June 1980.

[14] L. W. Pearson, "A ray representation of surface diffraction by a multilayer cylinder," *IEEE Trans. Antennas Propagat.*, vol. AP-35, pp. 698–707, June 1987.

[15] B. K. Singaraju, D. V. Giri, and C. E. Baum, "Further developments in the application of contour integration to the evaluation of the zeros of analytic functions and relevant computer programs," Math Note 42, U.S. Air Force Weapons Lab., Kirtland AFB, NM, 1976.

[16] K. Naishadham and L. B. Felsen, "Dispersion of wave guided along a cylindrical substrate-supertrate layered medium," *IEEE Trans. Antennas Propagat.*, vol. 41, pp. 304–313, Mar. 1993.

[17] M. Abramowitz and I. A. Stegun, Eds., *Handbook of Mathematical Functions*. New York; Dover, 1972.

[18] P. E. Hussar, "An AAPG surface diffraction formulation for advanced aircraft surfaces," DoD Joint Specrtrum Ctr., Annapolis, MD, Tech. Rep. JSC-TR-95-001, 1995.

Paul E. Hussar (M'92) was born in Washington, DC, on January 4, 1954. He received the B.S. degree in physics from the Massachusetts Institute of Technology, Cambridge, in 1975, and the M.S. (physics) and Ph.D. degrees (elementary particle physics) from the University of Maryland, College Park, in 1977 and 1982, respectively.

In 1983, he joined the staff of what is now the Department of Defense Joint Spectrum Center Support Group of the IIT Research Institute (IITRI), Annapolis, MD, where he currently holds the position of Engineering Science Advisor. His efforts at IITRI have been devoted to the application of high-frequency diffraction theory and antenna-array/adaptive-nulling theory to electromagnetic interference problems.

Dr. Hussar is a member of Phi Beta Kappa.